Photonuclear Fission from High Energy Electrons from Ultraintense Laser-Solid Interactions

T. E. Cowan,[1] A. W. Hunt,[5] T. W. Phillips,[1] S. C. Wilks,[1] M. D. Perry,[1] C. Brown,[1] W. Fountain,[3] S. Hatchett,[1]
J. Johnson,[4] M. H. Key,[1] T. Parnell,[3] D. M. Pennington,[1] R. A. Snavely,[1] and Y. Takahashi[2]
[1]*University of California, Lawrence Livermore National Laboratory, Livermore, California 94550*
[2]*University of Alabama, Huntsville, Alabama 35899*
[3]*George C. Marshall Space Flight Center, Huntsville, Alabama 35812*
[4]*Universities Space Research Association, Huntsville, Alabama 35806*
[5]*Harvard University, Cambridge, Massachusetts 02138*
(Received 23 March 1999)

A new regime of laser-matter interactions in which the quiver motion of plasma electrons is fully relativistic, with energies extending well above the threshold for nuclear processes, is studied using a petawatt laser system. In solid target experiments with focused intensities exceeding 10^{20} W/cm^2, high energy electron generation, hard bremsstrahlung, and nuclear phenomena have been observed. We report here a quantitative comparison of the high energy electrons and the bremsstrahlung spectrum, as measured by photonuclear reaction yields, including the photoinduced fission of ^{238}U.

PACS numbers: 52.40.Nk, 25.20.–x, 25.85.Jg, 52.60.+h

A new regime of strongly relativistic plasma physics has been opened to broad experimental study in recent years by the development of intense multiterawatt short-pulse lasers [1]. Nonlinear and relativistic effects have been observed when the product of the laser intensity times the square of the wavelength exceeds $\sim 10^{18}$ (W/cm^2)μm^2, at which point the quiver energy of the electrons in the laser focus becomes comparable to the electron rest mass [2]. In relativistic laser-solid interactions, very large numbers of electrons in this energy range have been measured [3], and their energy spectrum has been shown to resemble a relativistic Maxwellian distribution with an effective temperature,

$$E_{\mathrm{avg}} = mc^2[1 + 2U_p/mc^2]^{1/2}, \qquad (1)$$

which scales with the ponderomotive potential of the laser, $U_p[\mathrm{eV}] = 9.33 \times 10^{-14} I[\mathrm{W/cm^2}]\,\lambda^2[\mu\mathrm{m}]$. Effective electron temperatures of several hundred keV have also been inferred in other laser-solid experiments from the measurement of x ray [4] and bremsstrahlung [5] generation, and from evidence of photodissociation of ^{2}H performed with CO_2 lasers [6]. Small numbers of much higher energy electrons, up to 100 MeV, have been observed only in underdense laser-plasma experiments by laser wakefield acceleration [7] where $\sim$100 GV/m acceleration gradients could be sustained over $\sim$mm distances.

With the recent advent of petawatt-class lasers [8], capable of achieving 10^{15} W with focused intensities above 10^{20} W/cm^2 at $\lambda = 1$ μm, electrons with energies in excess of $\sim$10 MeV, and comparable to typical nucleon binding energies, can be produced in large numbers from the interaction of the laser with a solid target. At the Lawrence Livermore National Laboratory Petawatt laser facility we have observed laser-driven photonuclear processes throughout the periodic table [9–12]. In this Letter we present a direct comparison of the measured distribution of high energy electrons to the bremsstrahlung spectrum deduced from photonuclear reaction yields, including the observation of laser-driven nuclear fission.

In the present work, 260 J of 1.05 μm laser light, in a 450 fs long pulse, was focused onto a solid gold target, after being reflected from a plasma mirror (Fig. 1 inset). The focal spot size was $\sim$20 μm, producing an average intensity of greater than 10^{20} W/cm^2, corresponding to a ponderomotive energy of $\sim$3 MeV [from Eq. (1)]. A lower intensity prepulse of $<$100 mJ was focused on the target $\sim$2 ns prior to the main pulse. The prepulse created a plasma at the target surface, which from a plasma hydrodynamic calculation [13] we expect to have undergone a two-dimensional expansion with a rapidly decreasing plasma density extending away from the target. The density scale length is estimated to be $\sim$50 μm, in which the main laser pulse experiences relativistic self-focusing

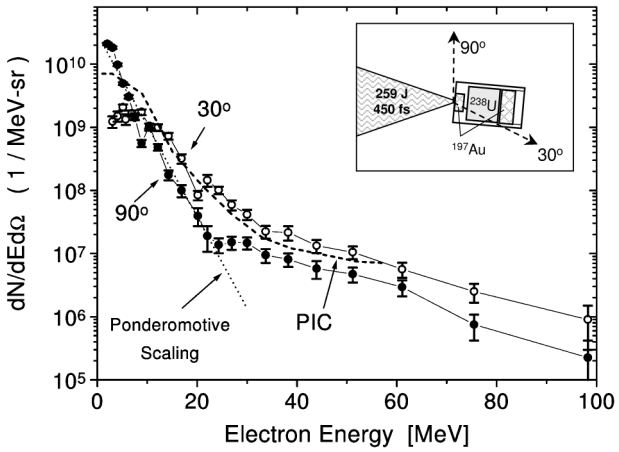

FIG. 1. Measured energy distributions of electrons ejected from the target at 30° (open circles) and 90° (solid circles) with respect to the incident laser pulse (as shown in the inset). Dashed curve shows expectation from Eq. (1), for the laser acting exclusively on the critical-density surface. Solid curve shows results of PIC simulations described in text.

or filamentation [14]. The gold target was mounted on a cylindrical copper sample holder, which contained an additional quantity of ^{197}Au (0.3 g) and ^{238}U (1.2 g). Following the laser shot, the target assembly was placed in a time-resolved gamma-ray spectrometer to search for nuclear activation from photoneutron and photofission reactions in the copper, gold, and uranium.

High energy electrons escaping the target during the laser pulse were measured directly in two magnetic spectrometers positioned at angles of 30° and 90° with respect to the propagation direction of the incident laser. As indicated in Fig. 1 (inset), the 30° spectrometer measured electrons that had penetrated several mm through the target assembly, and had lost at least 3 MeV of kinetic energy. The target was tilted slightly so that the 90° spectrometer had a clear view of electrons emerging from the direct laser-plasma interaction. The permanent-magnet electron spectrometers are described elsewhere [9]. They subtended an angular range of 3 mrad, with a solid angle of 7.0×10^{-6} sr. The electrons were recorded in nuclear emulsion track detectors, and identified under microscopic examination of the developed emulsions by the topography of their tracks of exposed silver bromide grains. The electron energy distribution was determined by point measurement of the track density, corrected for the energy dispersion, as a function of position along the 2 to 100 MeV usable range of the detection plane.

In this and in prior petawatt shots [9–12], electrons of energy up to 100 MeV have been observed in a broadly decreasing spectrum versus energy with multiple exponential slope components. Figure 1 shows a representative electron energy spectrum taken on another shot having identical laser parameters and for which the photoneutron activation yields in the copper and gold materials were essentially identical to the shot including the ^{238}U sample. The flux of electrons observed below ~10 MeV in the 30° spectrometer is suppressed by an order of magnitude or more by scattering through the target material. The low energy portion of the electron spectrum is largely consistent with the direct ponderomotive scattering of electrons out of the laser focus, and resembles a Maxwellian with a ~3 MeV mean energy [2]. The high energy tail extending up to 100 MeV can be attributed to acceleration processes in the subcritical density pre-formed plasma, as discussed later in this paper.

After the laser shot, the target was removed from the petawatt target chamber and transported to a shielded high purity germanium gamma-ray spectrometer for a time dependent measurement of the residual nuclear activation gamma rays produced by the laser shot. The entire target assembly had been measured prior to the laser shot as well, to directly determine the spectrum of room background and ^{238}U decay-chain gamma rays present in the target material used. Figure 2a shows a portion of the nuclear gamma-ray energy spectrum comparing data from before and after the petawatt shot. A large collection of additional

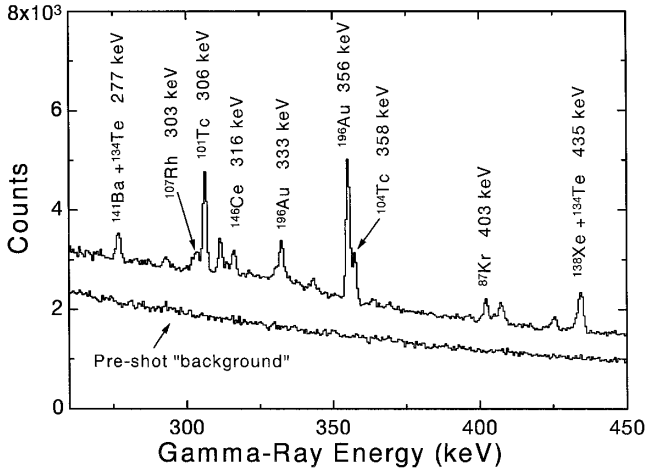

FIG. 2. Energy distribution of gamma rays emitted from the petawatt target assembly, measured before and after the laser shot (as marked).

lines was observed after the shot, including several that we had previously detected from photoneutron reactions in the Au and Cu target material [9–12]. For example, the gamma-ray lines at 333 and 356 keV are from the radioactive decay of ^{196}Au (to ^{196}Pt) which was produced by $^{197}\mathrm{Au}(\gamma, n)^{196}\mathrm{Au}$, from high energy bremsstrahlung photons above the 8.05 MeV photoneutron reaction threshold energy. An important aspect of this measurement technique is that we accumulated gamma-ray energy spectra in narrow time intervals following the shot. This allowed us to identify many short-lived reaction products by both their gamma-ray line energy and their characteristic decay half-life. For example, by the lifetime analysis of the 511 keV positron annihilation gamma-ray line observed after the shot, we were able to identify the presence of the positron emitters, ^{64}Cu (12.7 h) and ^{62}Cu (9.7 min). These were produced by photoneutron reactions in the naturally occurring copper isotopes present in the target assembly, $^{65}\mathrm{Cu}(\gamma, n)^{64}\mathrm{Cu}$ and $^{63}\mathrm{Cu}(\gamma, n)^{62}\mathrm{Cu}$.

The time-resolved gamma-ray information was used to identify decay products from the photoinduced fission of ^{238}U [15]. The nuclides we have identified by their gamma-ray line energies and half-lives include ^{87,88}Kr, ^{92,93}Sr, ^{93,94,95}Y, ^{101,104}Tc, ^{105}Ru, ^{107}Rh, ^{128}Sb, ^{128}Sn, ^{134}Te, ^{135}I, ^{138}Xe, ^{138}Cs, ^{141}Ba, and ^{146}Ce. The direct contribution to the yield of a given nuclide by the fission process was obtained from the total yield, after making corrections for contributions from other decay chains. We have compared our data to previous measurements [16] of these yields for specific nuclides from photofission of ^{238}U with accelerator-based bremsstrahlung beams. As shown in Fig. 3, the mass distribution of the fission products lies upon the usual double-humped distribution, which results from the large deformation of the ^{238}U parent. By normalizing to an empirical 6% cumulative yield per fission [16] for the ^{135}I daughter, we estimate a

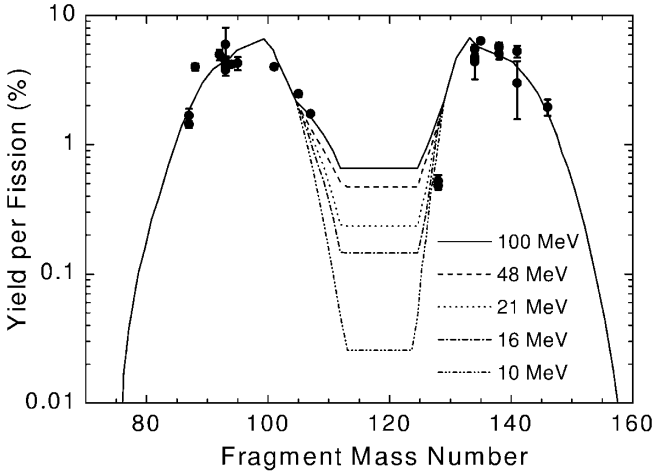

FIG. 3. Mass distribution of fission fragments detected. Curves show mass yield versus bremsstrahlung end-point energy for accelerator-based measurements.

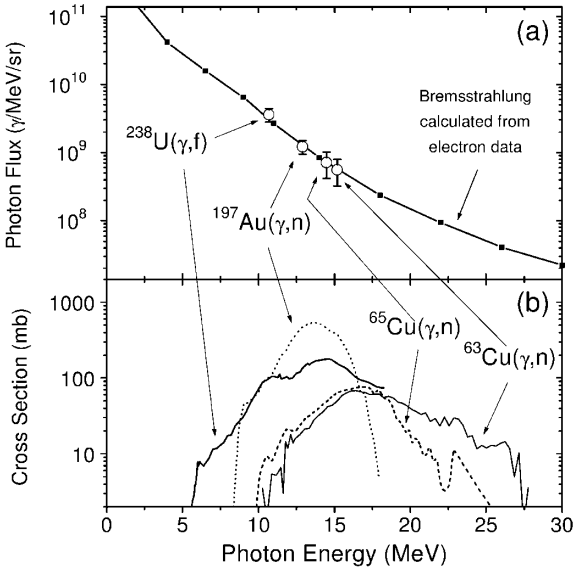

FIG. 4. (a) Comparison of photonuclear reaction yields to the bremsstrahlung photon distribution [(photons/MeV)/sr at 0°], calculated from the measured electron spectra (Fig. 1). (b) Energy-dependent photonuclear cross sections.

total yield in this experiment of $(1.8 \pm 0.2) \times 10^7$ fission events. We can assign this fission yield almost entirely to photofission, $^{238}\mathrm{U}(\gamma, f)$, as opposed to fission induced by neutrons from the photonuclear (γ, n) or from charged particle (p, xf) reactions by ion acceleration in the target plasma [6]. We determined this from the yield of ^{198}Au produced in the target by neutron capture and from the ratio of the (γ, f) and (n, f) cross sections in ^{238}U and the nonobservation of other proton induced reactions in the Au target.

Photofission and photoneutron reactions have different gamma-ray threshold energies, which can be used to measure the energy distribution of bremsstrahlung photons produced by the plasma electrons, over the photon energy range of ~5 to 20 MeV. This is a particularly valuable technique because it covers the energy range characteristic of the radiation processes present in ultraintense laser-plasma interactions. In this range simpler photon absorption techniques (see, e.g., [5]) are insensitive because the photon energy is above the Compton minimum in the mass attenuation coefficient. The photoneutron (γ, n) threshold energy is characteristic of the neutron binding energy in the target nuclide (e.g., ~8 MeV in ^{197}Au, and ~10 MeV in Cu). Whereas the photofission threshold in $^{238}\mathrm{U}(\gamma, f)$ is only 5 MeV because the process requires only a modest excitation to deform the ^{238}U nucleus into its fissioning transitional state [16].

Figure 4 presents a comparison of the yields of ^{238}U photofission, and ^{197}Au and ^{63}Cu photoneutron reactions in this experiment, to the bremsstrahlung yield calculated from the measured electron energy distribution. A variety of assumptions was made regarding the angular distribution of the high energy electrons which enter into the radiation transport calculation. These and other nuclear excitation experiments at the Petawatt suggest that the electron distribution can contain isolated "jetlike" features and other anisotropies [17,18]. However, when averaged over a broad angular range, the bulk of the intensity is forward directed in a broad cone. For the purposes of this comparison, we developed a self-consistent description of the electron energy and angle distributions. We iteratively assumed an initial energy distribution constant over a given cone angle, transported it through the target using the ITS Monte Carlo package [19], and compared it to the observed electron spectrum at 30°. We were able to obtain a good empirical match to the measured electron distribution, which gave an effective energy slope of the exponentially decreasing electron distribution. From this we calculate the energy-weighted nuclear reaction yield, expected for photofission and photoneutron reactions [12,20]. Even though the fission cross section is significantly smaller than the photoneutron cross section for ^{197}Au at their respective peaks, the very steep bremsstrahlung energy distribution greatly enhances the importance of the fission cross section just above its much lower 5 MeV threshold. The weighted-average energy for the $^{238}\mathrm{U}(\gamma, f)$ fission yield is well below the average for $^{197}\mathrm{Au}(\gamma, n)$. The measured fission and photoneutron reaction yields are in very good agreement with the expectations from the measured electron distribution. Taken together, the $^{238}\mathrm{U}(\gamma, f)$, $^{197}\mathrm{Au}(\gamma, n)$, and $^{63,65}\mathrm{Cu}(\gamma, n)$ reactions span a large range of effective nuclear excitation energy and hence provide good sensitivity for directly measuring the slope and total intensity of the bremsstrahlung energy spectrum from 5 to 20 MeV.

In future experiments, the identification of more fragment masses in the valley between the mass peaks would provide a complementary determination of the effective slope of the hard bremsstrahlung energy spectrum. The relative absence of fragments in this valley is consistent

with our rather soft bremsstrahlung spectrum. The valley fills in with increasing bremsstrahlung end-point energy, as seen in accelerator-based photofission measurements (Fig. 3), which reflects the relative importance of barrier penetration to the elongated transitional state in the deformed ^{238}U nucleus. The very intense, short-pulse nature of the radiation burst generated in petawatt laser-solid interactions might also provide useful opportunities for nuclear research in the future, perhaps for total photofission cross-section measurements on small samples, or for measuring the population of isomeric states having lifetimes in a range inconvenient for accelerator- or reactor-based experiments.

The observation of photonuclear reactions in this experiment is in quantitative agreement with the production of a large number of $\geq$10 MeV electrons, well in excess of the $\sim$3 MeV ponderomotive energy scale predicted by Eq. (1) (see Fig. 1). This suggests electron acceleration in the underdense preformed plasma, for example, stimulated Raman forward scatter [21] and self-modulated wakefield acceleration [22]. In addition, 3D and magnetic field effects can also create energetic electrons [23]. We performed 2D particle-in-cell (PIC) simulations in order to identify the principal acceleration mechanisms present in these experiments. As input, we used the results of the hydrocalculation [13] to estimate the preformed plasma created by the laser prepulse. We found that for a wide range of prepulse energies (40–90 mJ) there should be a relatively broad region of near critical-density plasma $[(0.1-1.0)n_{\mathrm{cr}}]$ for $\sim$50 μm in front of the original solid target surface. We assumed a laser intensity of 10^{20} W/cm^2 in a 3.5 μm diameter focus, with periodic transverse boundary conditions. This allowed us to simulate the filamentation and self-focusing of the incident $\sim$20 μm beam in the preformed plasma relevant to the electron acceleration mechanisms. Direct simulation of the entire experimental interaction region for the full pulse duration is presently computationally prohibitive. The resulting electron energy spectrum extends up to an energy of 60 MeV. After accounting for the transport of the electrons through the target material [19], the predicted electron distribution is in reasonably good agreement with the experimentally measured spectrum (as shown in Fig. 1) over most of the energy range responsible for the hard bremsstrahlung production.

In summary, we have extended the study of relativistic laser-matter interactions into a range where the electron quiver energies can be greater than several MeV, and hybrid laser-plasma acceleration mechanisms may be able to produce large numbers of electrons well above the threshold for causing nuclear reactions. In addition to the generation of high energy electrons up to $\sim$100 MeV, we have observed photoneutron reactions and nuclear fission in ^{238}U, induced by the bremsstrahlung produced throughout the target assembly. The low photofission threshold extends the range over which one can use nuclear activation techniques to characterize hard radiation processes in laser-plasma experiments. We find that the photonuclear reaction yields are in good agreement with our direct measurement of the energy spectrum of high energy electrons, and they can be used to characterize the energy distribution, yield, and average angular distribution of relativistic electrons produced in ultrarelativistic laser-solid interactions. Next generation experiments are in progress which use nuclear activation to determine the detailed angular distribution of hard bremsstrahlung produced in ultraintense laser plasmas [18].

We would like to acknowledge valuable contributions by many of our Petawatt collaborators and the expert assistance of W. S. Patterson and the Nova staff in fielding these experiments. This work was performed under the auspices of the U.S. Department of Energy by the Lawrence Livermore National Laboratory under Contract No. W-7405-Eng-48.

[1] M. D. Perry and G. Mourou, Science **264**, 917 (1994).
[2] S. C. Wilks *et al.*, Phys. Rev. Lett. **69**, 1383 (1992).
[3] G. Malka and J. L. Miquel, Phys. Rev. Lett. **77**, 75 (1996).
[4] K. B. Wharton *et al.*, Phys. Rev. Lett. **81**, 822 (1998).
[5] J. D. Kmetec *et al.*, Phys. Rev. Lett. **68**, 1527 (1992).
[6] N. K. Sherman, N. H. Burnett, and G. D. Enright, in *New Developments in Particle Acceleration Techniques*, edited by S. Turner (CERN, Geneva, 1987), Vol. 2, p. 675.
[7] A. Modena *et al.*, Nature (London) **377**, 606 (1995).
[8] M. D. Perry *et al.*, Opt. Lett. **24**, 160 (1999).
[9] T. E. Cowan *et al.*, in *Lasers '97*, edited by J. J. Carroll and T. A. Goldman (STS Press, McLean, VA, 1998), p. 882; T. E. Cowan *et al.*, Laser Part. Beams **17**, 4 (1999).
[10] M. D. Perry *et al.*, Rev. Sci. Instrum. **70**, 265 (1999).
[11] M. H. Key *et al.*, Phys. Plasmas **5**, 1966 (1998).
[12] T. W. Phillips *et al.*, Rev. Sci. Instrum. **70**, 1213 (1999).
[13] K. Estabrook, LASNEX simulation (private communication).
[14] M. Borghesi *et al.*, Phys. Rev. Lett. **78**, 879 (1997).
[15] A. W. Hunt *et al.* (to be published).
[16] S. Kahane and A. Wolf, Phys. Rev. C **32**, 1944 (1985); E. Jacobs *et al.*, Phys. Rev. C **19**, 422 (1979); H. Thierens *et al.*, Phys. Rev. C **14**, 1058 (1976).
[17] R. A. Snavely *et al.* (to be published).
[18] M. Stoyer *et al.* (to be published).
[19] J. A. Halbleib, Nucl. Sci. Eng. **92**, 338 (1986).
[20] B. L. Berman, At. Data Nucl. Data Tables **15**, 319 (1975).
[21] K.-C. Tzeng *et al.*, Phys. Rev. Lett. **79**, 5258 (1997).
[22] E. Esarey *et al.*, Phys. Rev. Lett. **80**, 5552 (1998).
[23] A. Pukov *et al.*, Phys. Rev. Lett. **76**, 3975 (1996).